

QCD Standard Model measurements with the ATLAS Detector

Matthew Feickert
(on behalf of the ATLAS Collaboration)

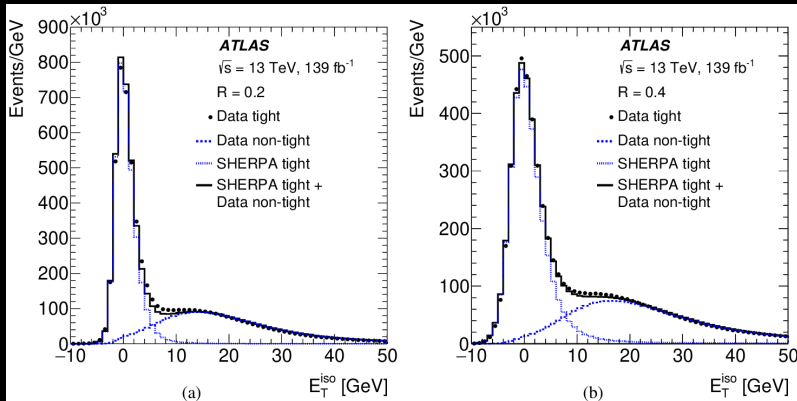
University of Wisconsin-Madison

Lake Louise Winter Institute 2023
February 20th, 2023

- ▶ LHC datasets offer truly unique environment for probing QCD
 - ▶ Tests of perturbative QCD (pQCD) predictions at high scales
 - ▶ Extracting strong coupling constant $\alpha_s(Q)$ and its running
 - ▶ Differential cross-section measurements over multiple orders of magnitude
- ▶ Huge dataset and precise object reconstruction enable increased precision and more granular measurements
 - ▶ Full ATLAS Run-2 dataset ($L = 139 \text{ fb}^{-1}$) enables precise tests of QCD
 - ▶ Boon for novel techniques sensitive to difficult to model remote areas of QCD phase space
- ▶ Focusing on 3 recent results from ATLAS today:
 - ▶ Inclusive-photon production and its dependence on photon isolation [ATLAS-STDM-2018-39] (arXiv:2302.00510)
 - ▶ Determination of the strong coupling using Transverse Energy-Energy Correlations (TEEC) in multijet events [ATLAS-STDM-2018-51] (arXiv:2301.09351)
 - ▶ Measurements of multijet event isotropies using optimal transport [ATLAS-CONF-2022-056]

Inclusive-Photon Production and its Dependence on Photon Isolation

E_T^{iso} distributions for photon candidates in data for background determination [ATLAS-STDM-2018-39] (arXiv:2302.00510)



New! results from ATLAS using the full Run-2 data set (139 fb^{-1})

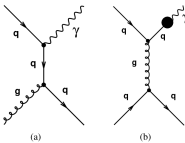
Inclusive photon

[ATLAS-STDM-2018-39] (arXiv:2302.00510)

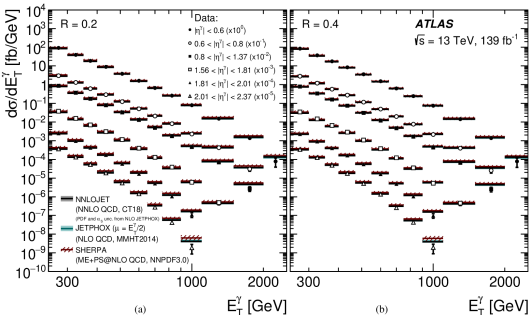


- ▶ Production of prompt (not secondaries from hadron decays) photons at high p_T in $p\text{-}p$ collisions, $pp \rightarrow \gamma + X$, provides a testing ground for pQCD in a cleaner environment compared to jet production, as it is less affected by hadronisation effects
- ▶ Results compared to JETPHOX, SHERPA, NNLOjet MC simulations with different PDF sets for NLO and NNLO comparisons to differential cross sections

Program	Order in α_s	Fragmentation	Parton shower	Isolation method	PDF	Particle level
JETPHOX	NLO	yes	no	fixed cone	- MMHT2014 - CT18 - NNPDF3.1 - HERAPDF2.0 - ATLASpdf21	no
SHERPA 2.2.2	NLO for $\gamma + (1, 2)\text{-jet}$ LO for $\gamma + (3, 4)\text{-jet}$	no	yes	hybrid	NNPDF3.0	yes
NNLOJET	(N)NLO	yes	no	fixed cone	CT18NNLO	no

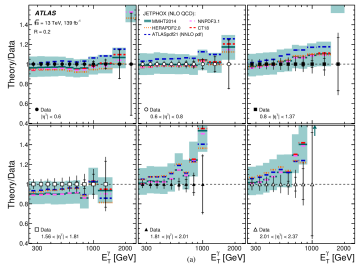


Leading order contributions: direct process and fragmentation process

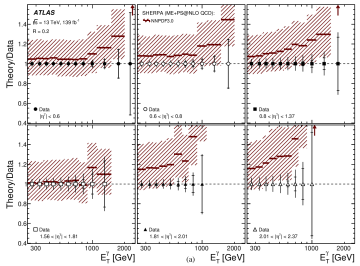


Differential measurements span nearly 6 order of magnitude

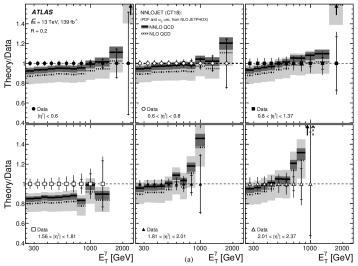
Measurements have potential to further constrain PDFs within global NNLO QCD fit



JETPHOX



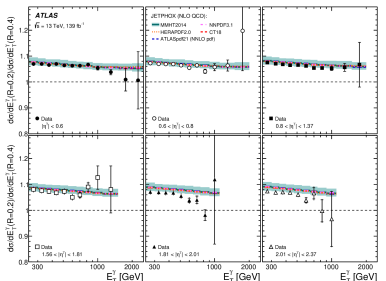
Sherpa NLO



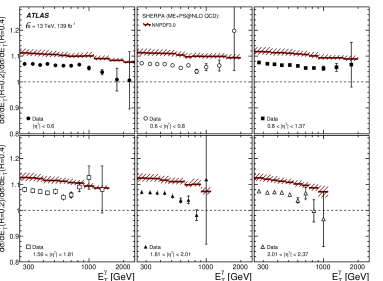
NNLOjet

- ▶ Ratio of the NLO (or NNLO) pQCD calculations from theory and the measured differential cross sections for inclusive isolated-photon production with $R = 0.2$ as functions of E_T^γ in different η^γ regions
- ▶ Experimental systematic uncertainties smaller than theoretical uncertainties over the full investigated phase space
- ▶ NNLOjet NNLO calculation (solid line) has sizeable reduction of the scale uncertainty!

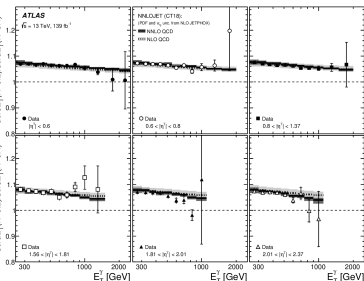
Ratios provide very stringent test of pQCD, with significantly reduced experimental and theoretical uncertainties



JETPHOX



Sherpa NLO

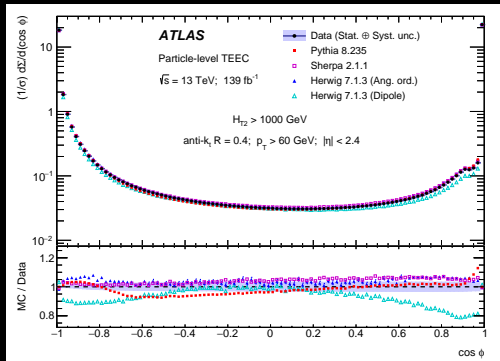


NNLOjet

- ▶ Measured ratios of the differential cross sections for inclusive isolated-photon production for $R = 0.2$ (numerator) and $R = 0.4$ (denominator) as functions of E_T^γ in different η^γ regions.
- ▶ Uncertainty bars show combined statistical and systematic. Shaded bands show theoretical uncertainties.

Determination of the strong coupling using Transverse Energy-Energy Correlations in multijet events

Comparison between the data and the MC expectations for the TEEC for the inclusive H_{T2} bin [ATLAS-STDM-2018-51] (arXiv:2301.09351)



results from ATLAS using the full Run-2 data set (139 fb^{-1})

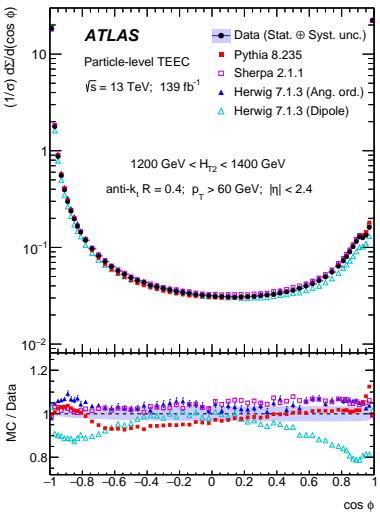
- ▶ Determination of the strong coupling using Transverse Energy-Energy Correlations (TEEC) in multijet events
- ▶ E_T -weighted distribution of the $\Delta\phi$ between jet pairs

$$\frac{1}{\sigma} \frac{d\Sigma}{d \cos \phi} = \frac{1}{\sigma} \sum_{ij} \int \frac{d\sigma}{dx_{T_i} dx_{T_j} d \cos \phi} x_{T_i} x_{T_j} \cos \phi = \frac{1}{N} \sum_{A=1}^N \sum_{ij} \frac{E_{T_i}^A E_{T_j}^A}{\left(\sum_k E_{T_k}^A \right)^2} \delta(\cos \phi - \cos \phi_{ij})$$

- ▶ $\cos \phi = -1$: back-to-back jets (dijet-like)
- ▶ $\cos \phi = 1$: collinear jets (sensitive to splittings, soft effects)
- ▶ Jet radius effect seen in kink at $\cos \phi \approx 0.92$

Generator	ME order	ME partons	PDF set	Parton shower	Scales μ_R, μ_F	$\alpha_s(m_Z)$
PYTHIA 8	LO	2	NNPDF 2.3 LO	p_T -ordered	$(m_{T3}^2 \cdot m_{T4}^2)^{\frac{1}{2}}$	0.140
SHERPA	LO	2,3	CT14 NNLO	CSS (dipole)	$H(s, t, u) [2 \rightarrow 2]$ $CMW [2 \rightarrow 3]$	0.118
HERWIG 7	NLO	2,3	MMHT2014 NLO	Angular-ordered Dipole	$\max(p_{Ti})_{i=1}^N$	0.120

Results compared to PYTHIA8, SHERPA, HERWIG7



Comparison of data and MC expectations for TEEC

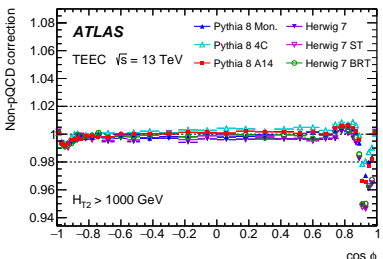
- ▶ Determination of the strong coupling using Transverse Energy-Energy Correlations (TEEC) in multijet events
- ▶ E_T -weighted distribution of the $\Delta\phi$ between jet pairs

$$\frac{1}{\sigma} \frac{d\Sigma}{d \cos \phi} = \frac{1}{\sigma} \sum_{ij} \int \frac{d\sigma}{dx_{T_i} dx_{T_j} d \cos \phi} x_{T_i} x_{T_j} \cos \phi = \frac{1}{N} \sum_{A=1}^N \sum_{ij} \frac{E_{T_i}^A E_{T_j}^A}{\left(\sum_k E_{T_k}^A \right)^2} \delta(\cos \phi - \cos \phi_{ij})$$

- ▶ $\cos \phi = -1$: back-to-back jets (dijet-like)
- ▶ $\cos \phi = 1$: collinear jets (sensitive to splittings, soft effects)
- ▶ Jet radius effect seen in kink at $\cos \phi \approx 0.92$

Generator	ME order	ME partons	PDF set	Parton shower	Scales μ_R, μ_F	$\alpha_s(m_Z)$
PYTHIA 8	LO	2	NNPDF 2.3 LO	p_T -ordered	$(m_{T3}^2 \cdot m_{T4}^2)^{\frac{1}{2}}$	0.140
SHERPA	LO	2,3	CT14 NNLO	CSS (dipole)	$H(s, t, u) [2 \rightarrow 2]$ CMW [2 → 3]	0.118
HERWIG 7	NLO	2,3	MMHT2014 NLO	Angular-ordered Dipole	$\max \{p_{Ti}\}_{i=1}^N$	0.120

Results compared to PYTHIA8, SHERPA, HERWIG7



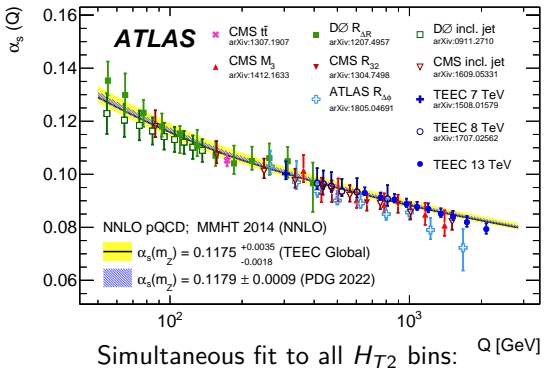
Non-perturbative corrections to the TEEC prediction for different tunes of PYTHIA8 and HERWIG7

TEEC at 13 TeV: Results

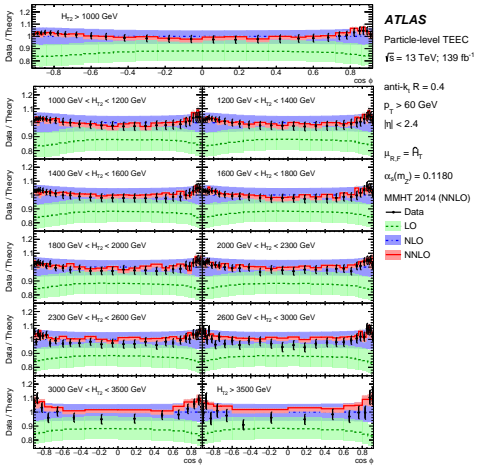
[ATLAS-STDM-2018-51] (arXiv:2301.09351)



- Used NNLO predictions to extract α_s at scale of Z pole mass and its running via χ^2 fit
- Able to probe α_s at high Q (up to 4 TeV) extending reach of previous measurements



$$\alpha_s(m_Z) = 0.1175 \pm 0.0006 (\text{exp.})^{+0.0034}_{-0.0017} (\text{theo.})$$



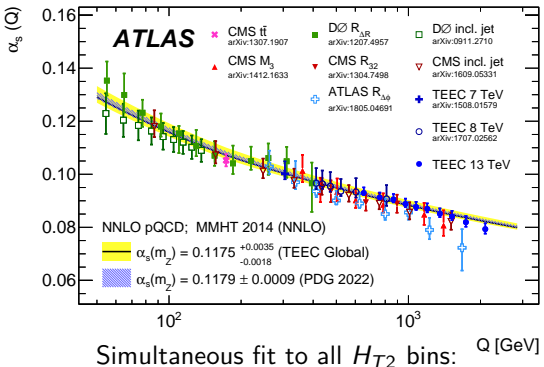
Ratios of theoretical predictions for the TEEC functions at LO and NNLO to the NLO calculations, shown with ratios of the data to NLO predictions.

TEEC at 13 TeV: Results

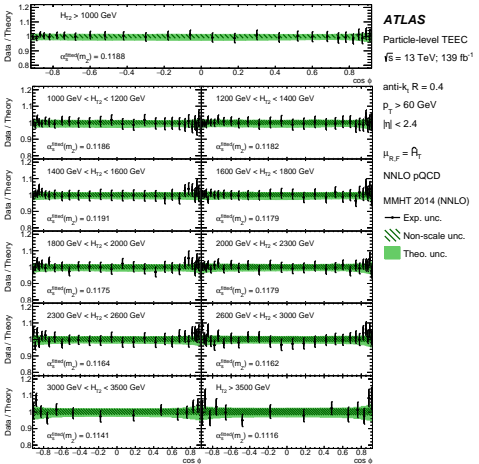
[ATLAS-STDM-2018-51] (arXiv:2301.09351)



- Used NNLO predictions to extract α_s at scale of Z pole mass and its running via χ^2 fit
- Able to probe α_s at high Q (up to 4 TeV) extending reach of previous measurements



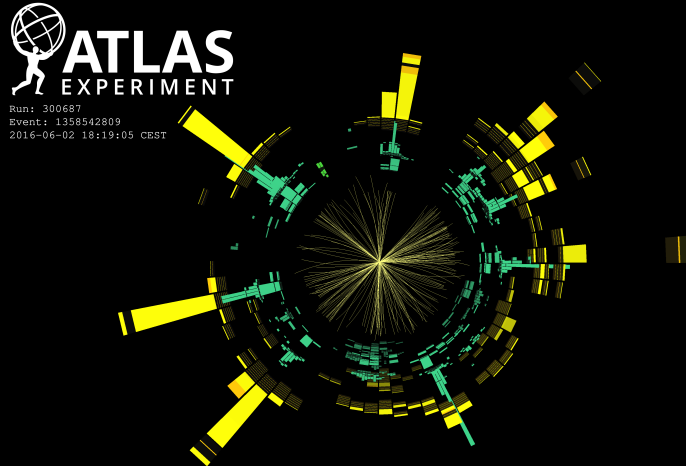
$$\alpha_s(m_Z) = 0.1175 \pm 0.0006 \text{ (exp.)}^{+0.0034}_{-0.0017} \text{ (theo.)}$$



Theory uncertainties dominated by scale variations. JES systematic uncertainty next dominant, followed by MC modeling and JER uncertainties.

Measurements of multijet event isotropies using optimal transport with the ATLAS detector

Most isotropic event passing the analysis selection (ATLAS LHC Run-2 $N_{jet} = 12$ event) [ATLAS-CONF-2022-056]



Event Isotropies at 13 TeV

[ATLAS-CONF-2022-056]



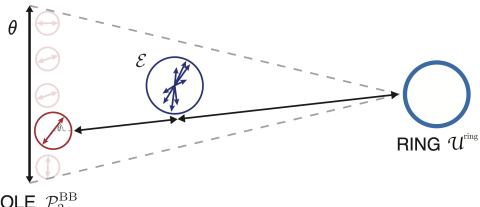
- ▶ Event shapes: observables used to describe the flow of energy in collider events
 - ▶ Designed to probe QCD radiation and compare event similarity to well-balanced dijet events
- ▶ Event isotropy: novel event shape defined as distance collider event is from a symmetric radiation pattern \mathcal{U} in the Wasserstein metric
 - ▶ Wasserstein distances given by Earth Mover's Distance (EMD) from optimal transport problems: **minimum required 'work'** to transport **one event to another** with equal energy by **movements of energy f_{ij}** from particle $i \leq M$ in one event to particle $j \leq M'$ in other
 - ▶ Infrared and colinear safe by construction!

$$\text{EMD}_{\beta} (\mathcal{E}, \mathcal{E}') = \min_{\{f_{ij} > 0\}} \sum_{i=1}^M \sum_{j=1}^{M'} f_{ij} \theta_{ij}^{\beta}$$

$$\sum_{i=1}^M f_{ij} = E'_j, \quad \sum_{i=1}^{M'} f_{ij} = E_i, \quad \sum_{i=1}^M \sum_{j=1}^{M'} f_{ij} = \sum_{i=1}^M E_i = \sum_{i=1}^{M'} E_j = E_{\text{tot}}$$

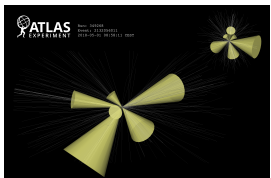
θ_{ij} : pairwise distance “ground measure”, $\beta > 0$ (here 2)

$$\mathcal{I}(\mathcal{E}) = \text{EMD}(\mathcal{E}, \mathcal{U})$$

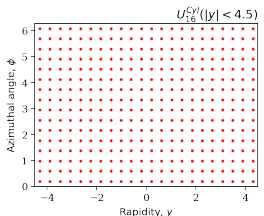


EMD of event \mathcal{E} to the manifold of two-particle back-to-back events ($\mathcal{P}_2^{\text{BB}}$) and to uniform ring-like geometry with $N = 128$ reference particles

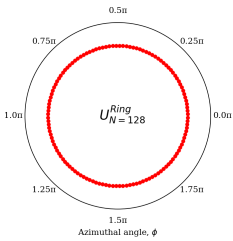
Geometry	Energy Weight	Ground Measure	Radiation Pattern \mathcal{U}
Cylinder	$w_i^{\text{cyl}} = p_{Ti}/p_{T\text{tot}}$	$\theta_{ij}^{\text{cyl}} = \frac{12}{\pi^2 + 16y_{\max}^2} (y_{ij}^2 + \phi_{ij}^2)$	$U_{N=16}^{\text{cyl}} (y < y_{\max})$
Ring	$w_i^{\text{ring}} = p_{Ti}/p_{T\text{tot}}$	$\theta_{ij}^{\text{ring}} = \frac{\pi}{\pi - 2} (1 - \cos \phi_{ij})$	$U_{N=128}^{\text{ring}}$
Ring (Dipole)	$w_i^{\text{ring}} = p_{Ti}/p_{T\text{tot}}$	$\theta_{ij}^{\text{ring}} = \frac{1}{1 - \frac{1}{\sqrt{3}}} (1 - \cos \phi_{ij})$	$U_{N=2}^{\text{ring}}$



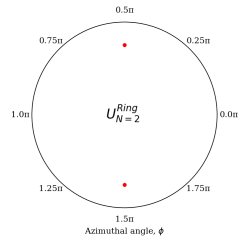
Event \mathcal{E} with $N_{\text{jet}} = 6$



$$\mathcal{I}_{\text{Cyl}}^{16} = \text{EMD}_2 (\mathcal{E}, \mathcal{U}_{16}^{\text{cyl}})$$



$$\mathcal{I}_{\text{Ring}}^{128} = \text{EMD}_2 (\mathcal{E}, \mathcal{U}_{128}^{\text{Ring}})$$



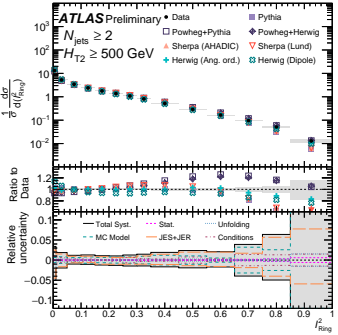
$$\mathcal{I}_{\text{Ring}}^2 = \text{EMD}_2 (\mathcal{E}, \mathcal{P}_2^{\text{BB}})$$

Event Isotropies at 13 TeV: Results

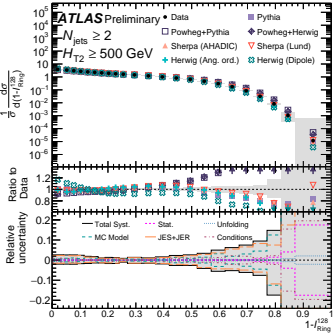
[ATLAS-CONF-2022-056]



- ▶ $\mathcal{I}_{\text{Ring}}^2$: MC generators roughly describe data
 - ▶ In isotropic region predictions with best agreement to data are NLO MC generators
- ▶ $1 - \mathcal{I}_{\text{Ring}}^{128}$: MC generators modeling of the data degrades at higher isotropic region
 - ▶ Generators disagree with each other at higher isotropy



Unfolded $\mathcal{I}_{\text{Ring}}^2$ compared to MC



Unfolded $1 - \mathcal{I}_{\text{Ring}}^{128}$ compared to MC

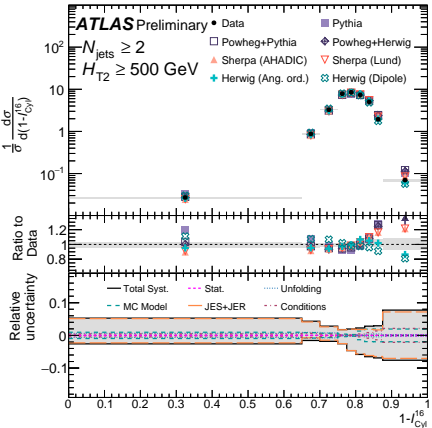
Left side of plot: more back-to-back
Right side of plot: more isotropic

Event Isotropies at 13 TeV: Results

[ATLAS-CONF-2022-056]



- ▶ $1 - \mathcal{I}_{\text{Cyl}}^{16}$: None of the MC generators describe the data well
 - ▶ Large differences between the parton shower models available in HERWIG
 - ▶ Complex observable!
- ▶ For all:
 - ▶ Agreement best in balanced, dijet-like configurations. Deteriorates in more isotropic configurations.
 - ▶ Useful observable for improving simulations at the LHC
 - ▶ Can be used in future Monte Carlo tuning campaigns and other QCD studies
 - ▶ Capable of exposing a remote piece of QCD phase space difficult to model and relevant to searches for physics beyond the Standard Model



Unfolded $1 - \mathcal{I}_{\text{Cyl}}^{16}$ compared to MC

Left side of plot: more back-to-back
Right side of plot: more isotropic

Conclusions

- ▶ The LHC provides rich environment for studying QCD
- ▶ Full ATLAS Run-2 dataset ($L = 139 \text{ fb}^{-1}$) allows for precision measurements of QCD and exploring novel techniques
- ▶ Measurements provide useful inputs for improving understanding of QCD
- ▶ Can be used in future Monte Carlo tuning campaigns and other studies of QCD (including PDF fits)
- ▶ Reminder: We're at the start of LHC Run 3!
 - ▶ More (better) measurements means improved modeling and smaller systematic uncertainties
 - ▶ More to come!



LHC long term schedule (updated January 2022)

- ▶ Single-photon high-level trigger with $E_T^\gamma > 140$ GeV and “loose” photon identification requirements
 - ▶ Trigger efficiency for photons with $E_T^\gamma > 250$ GeV close to 100%
- ▶ Offline selection from trigger data with:
 - ▶ at least one reconstructed primary vertex
 - ▶ at least two associated tracks of $p_T > 500$ MeV
 - ▶ consistent with the average beam-spot position

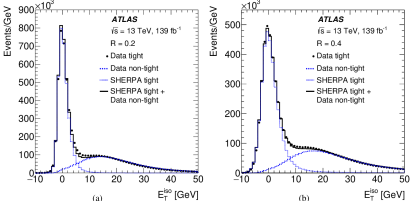
Inclusive photon: Background evaluation [ATLAS-STDM-2018-39] (arXiv:2302.00510)

- ▶ Multi-jet background from events passing event selection but failing tight photon identification and isolation requirements.
- ▶ ABCD method used
 - ▶ A: Signal region (tight, isolated)
 - ▶ B: Control region with non-isolated background events (contains tight and non-isolated photon candidates)
 - ▶ C: Control region with non-tight background events (contains isolated and non-tight photon candidates)
 - ▶ D: Control region with non-isolated and non-tight photon candidates

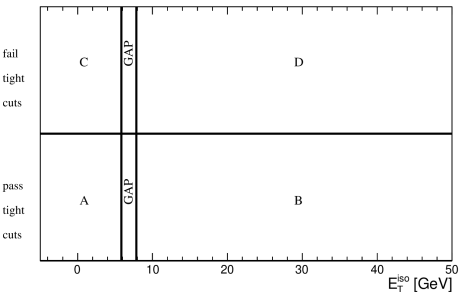
$$N_A^{\text{sig}} = N_A - R^{\text{bg}} \cdot \left(N_B - f_B N_A^{\text{sig}} \right) \cdot \frac{\left(N_C - f_C N_A^{\text{sig}} \right)}{\left(N_D - f_D N_A^{\text{sig}} \right)}$$

$$R^{\text{bg}} = \frac{N_A^{\text{bg}} \cdot N_D^{\text{bg}}}{N_B^{\text{bg}} N_C^{\text{bg}}}$$

- ▶ Signal purity: $P = N_A^{\text{sig}} / N_A > 90\%$



E_T^{iso} distributions for photon candidates in data



ABCD plane. Vertical lines correspond to the requirements on E_T^{iso} for $E_T^\gamma = 250$ GeV.

$$\frac{1}{\sigma} \frac{d\Sigma}{d \cos \phi} = \frac{1}{\sigma} \sum_{ij} \int \frac{d\sigma}{dx_{T_i} dx_{T_j} d \cos \phi} x_{T_i} x_{T_j} \cos \phi = \frac{1}{N} \sum_{A=1}^N \sum_{ij} \frac{E_{T_i}^A E_{T_j}^A}{(\sum_k E_{T_k}^A)^2} \delta(\cos \phi - \cos \phi_{ij})$$

- ▶ Valid for a sample of N multijet events, labelled by index A , with indices i, j, k running over all jets in a given event
- ▶ $E_T = E / \cosh y$
- ▶ $x_{T_i} = E_{T_i} / \sum_k E_{T_k}$: normalized transverse energy of jet i
- ▶ ϕ_{ij} : angle in the transverse plane between jet i and jet j
- ▶ Normalization to the total dijet cross-section, σ , ensures the integral of the TEEC function over $\cos \phi$ is unity

- ▶ χ^2 function:

$$\chi^2(\alpha_s, \boldsymbol{\lambda}) = \sum_{\text{bins}} \frac{(x_i - F_i(\alpha_s, \boldsymbol{\lambda}))^2}{\Delta x_i^2 + \Delta \xi_i^2} + \sum_k \lambda_k^2$$

where the theoretical predictions are varied according to

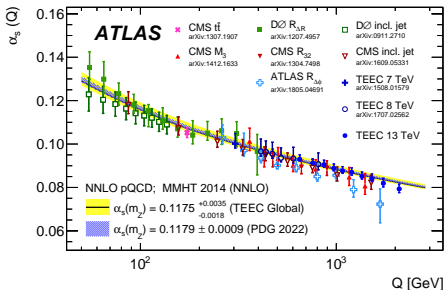
$$F_i(\alpha_s, \boldsymbol{\lambda}) = \psi_i(\alpha_s) \left(1 + \sum_k \lambda_k \sigma_k^{(i)} \right)$$

- ▶ α_s : $\alpha_s(m_Z)$
- ▶ x_i : value of the i -th point of the distribution as measured in data
- ▶ Δx_i : statistical uncertainty of x_i
- ▶ $\Delta \xi_i$: statistical uncertainty on theory predictions and uncorrelated modelling uncertainty
- ▶ $\psi_i(\alpha_s)$: analytical expression for dependence of each observable on the strong coupling constant for bin i
- ▶ λ_k : nuisance parameter associated with each source of experimental uncertainty
- ▶ $\sigma_k^{(i)}$: relative value of the k -th correlated source of systematic uncertainty in bin i

TEEC at 13 TeV: Why measure $\alpha_s(m_Z)$? [ATLAS-STDM-2018-51] (arXiv:2301.09351)



- ▶ The scale Q that $\alpha_s(Q)$ is measured at is ultimately an arbitrary choice
- ▶ Selecting the scale to be $Q = m_Z$ is practically useful as it allows comparisons to results from LEP
 - ▶ The value of Q for the TEEC 13 TeV points is chosen as half of the average of \hat{H}_T in each H_{T2} bin
- ▶ ~ 0.25 of total V production cross-sections at LHC come from processes beyond the Born level, and so depend on QCD coupling value. Calculating V production cross-sections at NNLO for varying $\alpha_s(m_Z)$ can derive value of $\alpha_s(m_Z)$ independent of other current extractions. [arXiv:1912.04387]



Comparison of the values of $\alpha_s(Q)$ determined from fits to the TEEC functions with the QCD prediction using the world average as input (hatched band) and the value obtained from the global fit (solid band).